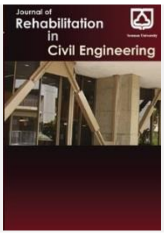

Journal of Rehabilitation in Civil Engineering

Journal homepage: https://civiljournal.semnan.ac.ir/

Time-Dependent Seismic Fragility of RC Moment Frames in Corrosive Environment Considering Concrete Quality

Mohammad Amiri [1]; Amirhossein Jafary [2,*]; Ali Khodam [2]; Mohsenali Shayanfar [1]; Sajad Zarei[1]

1. School of Civil Engineering, Iran Univ. of Science and Technology, Tehran, Iran
2. Department of Civil and Geomatics Engineering, Arak University of Technology, Arak, Iran
* Corresponding author: *ah.jafary@yahoo.com*

ARTICLE INFO

Article history:
Received: 19 October 2023
Revised: 08 June 2024
Accepted: 15 August 2024

Keywords:
Steel reinforcement corrosion;
Seismic performance;
Nonlinear static analysis;
Nonlinear dynamic analysis;
Fragility curve.

ABSTRACT

Corrosion of steel reinforcement in concrete is a common problem for reinforced concrete buildings in coastal regions. It can have significant impacts on the seismic performance of these buildings. Corrosion in reinforced concrete members can cause problems such as concrete cover removal, longitudinal cracks in concrete, and reduction of the cross-sectional area of steel reinforcements. Moreover, corrosion causes changes in the stress-strain curves of reinforcement steel, reducing its resistance. This study investigates the impact of corrosion on the seismic performance of a four-story concrete frame. In this context, moment-curvature curves for structural elements are first obtained, considering the impacts of corrosion on steel reinforcements and concrete. These curves are then used to model the plastic hinges under corrosion conditions in a nonlinear static (pushover) analysis of corroded RC frames. The pushover curves are then utilized to investigate the impacts of corrosion on the ductility and seismic capacity of the frame. The results show that corrosion significantly impacts the ductility of Reinforced Concrete (RC) frames and can increase the probability of collapse. Fragility curves obtained by incremental dynamic analysis show that the probability of exceeding damage states for structures with higher values of water-to-cement ratio in a corrosion scenario with columns exposed on two sides is significantly higher.

E-ISSN: 2345-4423

How to cite this article:
Amiri, M., Jafray, A., Khoddam, A., Shayanfar, M. A., & Zarei, S. (2025). Time-Dependent Seismic Fragility of RC Moment Frames in Corrosive Environment Considering Concrete Quality. Journal of Rehabilitation in Civil Engineering, 13(2), 75-93. https://doi.org/ 10.22075/jrce.2024.32075.1915

1. Introduction

Under normal conditions, concrete's high alkalinity (PH around 13) creates a thin, protective oxide layer on the steel reinforcement bars. This passive layer shields the steel from corrosion despite moisture and oxygen [1]. However, chloride ions or carbonation can degrade this protective layer, leaving the rebar vulnerable to corrosion in moisture [2–4]. The corrosion process leads to the formation of rust around the steel bars, with the volume of the rust exceeding the original steel volume by up to six times. This significant volume increase can induce cracking in the surrounding concrete. These cracks, in turn, facilitate further chloride ingress, accelerating the deterioration process [5,6]. Chloride-induced corrosion is particularly prevalent in harsh environments such as coastal regions and areas exposed to tidal waters [7]. Substandard materials, inadequate curing practices, and existing cracks in the concrete can all exacerbate rebar corrosion [8]. Such materials like GFRP rebars could overcome these drawbacks [9]. Studies on reinforced concrete (RC) structures in coastal areas have identified steel reinforcement corrosion as a significant contributor to concrete damage, significantly impacting concrete members' strength, stiffness, and ductility [10,11]. Two primary types of corrosion can occur in concrete members: 1) uniform corrosion affecting the entire bar surface, typically caused by carbonation, and 2) localized (pitting) corrosion resulting from chloride attacks [12–14]. Several detrimental effects become evident as the corrosion process progresses and oxidation products accumulate. These include the propagation of longitudinal cracks, a reduction in concrete compressive strength, loss of concrete cover, and decreased bond strength between rebars and the surrounding concrete [15,16]. Furthermore, corrosion can lead to a significant loss of cross-sectional area in the steel bars [17]. The changes in the stress-strain behavior of the steel due to corrosion can also reduce its strength [18]. These combined effects decrease the seismic capacity of concrete members, ultimately affecting the seismic performance of RC structures [19–21]. Numerous researchers have extensively studied the impact of corrosion on the bearing capacity and seismic performance of concrete members and RC structures [22].

Several studies have investigated the strength reduction caused by pitting corrosion in reinforcement. Ghanooni-Bagha et al. employed experimental and numerical approaches to analyze this phenomenon [23,24]. Their research emphasized the significance of the pitting radius-to-reinforcement diameter ratio on the load-bearing capacity, highlighting the role of stress concentration induced by pitting corrosion. Additionally, Biondini et al. explored the seismic performance of low-rise concrete frames, including a prefabricated one-story structure, by considering the deterioration of material properties due to corrosion from sulfates and chloride [10]. Similarly, Inci et al. evaluated the seismic performance of a four-story concrete structure with pitting corrosion in its columns, considering ten different corrosion scenarios [19]. Jafary et al. investigated the long-term effects of chloride-induced corrosion on RC structures using a 20-story special RC moment frame originally designed by Haselton [25]. Their study analyzed the frame's behavior 40 years after corrosion initiation, considering three different water-cement ratios. OpenSEES software was employed to conduct nonlinear analyses under both far-field and near-field ground motions from FEMA P-695. The results revealed that corrosion had a more significant impact on the frame's ductility than its overstrength capacity.

Additionally, the study found a higher likelihood of exceeding predefined damage states under near-field ground motions with non-pulse-like characteristics [25]. Yalciner et al. presented a case study examining the seismic performance of a 30-year-old school building exposed to a corrosive environment. They evaluated the effects of corrosion rate on the building's deformation by considering bond-slip between concrete and steel and the loss of cross-sectional area in the steel reinforcement bars for five different corrosion levels [26]. Afsar Dizaji et al. focused on the residual seismic capacity of reinforced concrete structures after experiencing corrosion damage [21]. Ghanooni-Bagha et al. employed moment-curvature diagrams to investigate the influence of corrosion on the capacity curves of reinforced concrete frames obtained through pushover analysis. They further assessed the achieved performance levels using incremental dynamic analysis [11]. Vaezi et al. studied the effects of changes in the mechanical properties of reinforcement due to carbonation corrosion. They modeled a 2D RC moment frame and investigated parameters such as seismic capacity and overall performance utilizing nonlinear static and incremental dynamic analysis [27].

This study uses probabilistic and deterministic computational methods to estimate the time when corrosion will start. The study also considers how the mechanical properties of structural elements degrade due to corrosion. This degradation is then factored into the moment-curvature relationships and the length of plastic hinges within nonlinear analyses. Two different corrosion scenarios are being considered: columns exposed to chloride attack on one side and columns exposed on both sides. For each scenario, three w/c ratios are considered. Pushover analyses are then performed for each of these six cases to investigate the impacts of corrosion on the frame's ductility and strength. Additionally, incremental dynamic analyses are conducted to obtain fragility curves and study the structure's seismic performance under different corrosion and w/c ratio scenarios.

2. Chloride-induced corrosion process

2.1. Chloride emissions in concrete

Chlorides can be incorporated into concrete during mixing through several sources. These include chloride-laden aggregates, salty mixing water, and specific additives. Additionally, chlorides can penetrate existing concrete through various pathways, such as windborne sea spray, de-icing salts applied during cold weather, or migration from underground water [8,28].

Due to limiting chloride-laden constituent materials in concrete construction, chloride ingress primarily occurs through environmental exposure. Fick's second law is commonly employed to model chloride diffusion into concrete, as shown in the following Equation [28]:

$$C(x,t)=Cs[1-\mathrm{erf}\left(\frac{x}{2\sqrt{Dt}}\right)] \quad (1)$$

Where C is the surface chloride concentration D (mol/m^3) is the diffusion coefficient (m^2/s), t is the time of exposure in terms of seconds, and x is the depth of interest from the concrete surface (m). *erf (.)* stands for error function that is defined as follows:

$$\mathrm{erf}(x)=\frac{1}{\sqrt{\pi}}\int_{-x}^{x} e^{-t^2}dt=\frac{2}{\sqrt{\pi}}\int_{0}^{x} e^{-t^2}dt \quad (2)$$

The concentration of chlorides on a concrete surface depends on several environmental factors, including regional topography, surface orientation relative to the chloride source, and distance from the coastline [29]. While some researchers posit an increase in surface chloride concentration over time [30], others assume a constant value [31,32]. For instance, McGee [32] proposed formulas relating surface chloride concentration to distance from the sea, as shown below (where d is the distance (km):

$$\begin{cases} Cs=2.95\ \left(\frac{kg}{m^3}\right) & d<0.1 \\ Cs=1.15-1.81Log_{10}(d) & 0.1<d<2.84 \\ Cs=0.03\left(\frac{kg}{m^3}\right) & d>2.84 \end{cases} \tag{3}$$

The diffusion coefficient (D) reflects concrete permeability and is influenced by the concrete mix design, such as the water-to-cement ratio and concrete type. Other influencing factors include curing conditions, compactness, environmental factors (e.g., temperature and moisture), and exposure time. The Papadakis et al. [33] model is considered one of the most effective models for the diffusion coefficient, demonstrating good agreement with laboratory results.

The following formula defines this chloride diffusion coefficient:

$$D=D_{H_2O}\times 0.15\frac{1+\rho_c\frac{W}{C}}{1+\rho_c\frac{w}{c}+\frac{\rho_c a}{\rho_a c}}\left(\frac{\rho_c\frac{w}{c}-0.85}{1+\rho_c\frac{w}{c}}\right)^3\quad\left(\frac{cm^2}{s}\right) \tag{4}$$

Where a/c is the ratio of aggregates to cement, D_{H_2O} is the initial chloride diffusion coefficient (1.6×10^{-5} cm^2/s for NaCl), and ρ_a and ρ_c Are respectively the aggregates and cement density.

2.2. Corrosion initiation

Chloride-induced corrosion initiates when the chloride concentration around the reinforcement bars exceeds a threshold value called the critical chloride concentration, C_{th} Stewart suggests 0.9 (kg/m^3) for the critical chloride concentration [34]. By placing the critical chloride concentration in Equation (1) and rewriting the Equation, the corrosion initiation time is deduced as follows:

$$t_{corr}=\frac{cover^2}{4D}\left[erf^{-1}\left(1-\frac{C_{th}}{C_s}\right)\right]^{-2} \tag{5}$$

Where $cover$ is the Concrete cover and C_{th} represents the critical chloride concentration.

2.3. Probabilistic and deterministic estimation of corrosion initiation time

This study calculates the corrosion initiation time for three high-quality concrete mixtures with water-to-cement (w/c) ratios of 0.40, 0.45, and 0.50. To isolate the impact of the w/c ratio on corrosion, we assume an equal initial seismic capacity for the concrete structures. Consequently, the concrete's initial compressive strength (before corrosion) is identical. As a result, only the diffusion coefficients and, subsequently, the corrosion initiation times will differ between the three w/c ratios.

A probabilistic and deterministic method has been employed to estimate the time for corrosion initiation within the structure. Using Equation 5 and disregarding uncertainties, the onset of corrosion time for water-to-cement ratios of 0.4, 0.45, and 0.5 has been obtained as ten years, 16 years, and 31 years, respectively. Table 1 summarizes the statistical properties of the parameters influencing corrosion initiation time. The final row of the table presents the estimated corrosion initiation times obtained using the proposed method for concrete structures with three different water-to-cement ratios. A 10% probability of corrosion initiation is used as the criterion for this estimation.

Table 1. Statistics of influencing parameters and corrosion initiation time.

Parameter	Cth (kg/m^3)	Cs (kg/m^3)	D (mm^2/year)			cover(mm)
			w/c= 0.4	w/c= 0.45	w/c= 0.5	
μ	0.90	2.95	38.3	73.8	144	50
COV	0.5	0.2	0.75	0.75	0.75	0.12
Distribution	LogNormal	LogNormal		LogNormal		Normal
Probability of corrosion (10%)			14 years	8 years	4 years	

Beyond differences in diffusion coefficient, the variations in corrosion initiation times presented in Table 1 can be attributed to several factors, including environmental conditions and distance from the sea. Other parameters, such as environmental conditions and distance from the sea, can affect corrosion initiation time and the diffusion coefficient. To avoid complicating the analysis by considering variations in structure exposure (e.g., distance from seismic sources) and environmental factors, this study focuses on the influence of emission factor changes on the initiation time and duration of corrosion processes. As seen in Table 1, the estimations of corrosion initiation time for concrete mix designs with w/c ratios of 0.40, 0.45, and 0.50 are 14, 8, and 4 years, respectively.

3. Impacts of corrosion on reinforced concrete elements

3.1. Reduced cross-section of bars

The most crucial deterioration resulting from corrosion is reducing the cross-sectional area of steel rebars. This reduces the capacity and ductility of concrete. This article used the pitting corrosion model by Val and Melchers to estimate the reduced cross-section of bars exposed to corrosion [17]. In this model, the radios of the pit in the bar at t is defined as follows:

$$p(t)=R\int_{t_{Corr}}^{t}\lambda(t)\,dt \tag{6}$$

Where λ is the corrosion rate at t, R is the factor to convert uniform corrosion into pitting corrosion, and t_{Corr} is the corrosion initiation time. According to the experimental studies, R varies from 4 to 8 [17]. Most researchers have assumed that the corrosion rate is constant in seismic fragility assessment and reliability analysis of RC structures [35–37]. However, experimental studies have shown that the corrosion rate changes over time [38–40]. Stewart et al. proposed a formula for the corrosion rate based on the data reported by Liu and Weyers [41].

This formula, which is widely used in the analysis of corroded RC structures, is as follows:

$$\lambda(t)=0.0116.i_{corr,0}.0.85.(t-t_{Corr})^{-0.29} \quad \left(\frac{mm}{year}\right) \tag{7}$$

Where t is time, t_{Corr} is the corrosion initiation time in a way that $t > t_{corr}$, and $i_{Corr,0}$ is the initial corrosion rate obtained using the following Equation:

$$i_{corr,0}=\frac{37.8(1-\frac{w}{c})^{-1.64}}{cover} \quad \left(\frac{\mu A}{cm^2}\right) \tag{8}$$

3.2 Cracks and change in concrete compressive strength due to corrosion

The high volume of rust products resulting from corrosion leads to cracks in the concrete, which reduces its compressive strength. Based on the study by [42], the reduction in concrete compressive strength depends on tensile strains developed in the concrete. They proposed the following Equation to estimate the reduced compressive strength of the cracked concrete:

$$f_c^*=\frac{f_c}{1+k\frac{\varepsilon_1}{\varepsilon_{c0}}} \tag{9}$$

Where k is a factor depending on the diameter and roughness of rebars, ε_{c0} is the concrete strain at the maximum compressive stress fc, and ε_1 that is the average tensile strain in the cracked concrete computed as follows:

$$\varepsilon_1=\frac{b_f-b_0}{b_0} \tag{10}$$

Where b_0 is the width of the pristine concrete element, and b_f is the width of the concrete member after cracks developed due to corrosion. The increase in concrete elements width due to cracking can be estimated by the following Equation:

$$b_f - b_0 = n_{bars}\, w_{cr} \quad (11)$$

In this Equation, nbars is the number of folded bars in the pressure zone, and w_{cr} is the width of the cracks developed in concrete due to corrosion from reinforcement. Ghanooni-Bagha et al. proposed a modified k factor in Eq (9) for reinforced concrete elements under corrosion based on the crack width [5]. Many studies are available on estimating the width of the cracks developed in concrete due to corrosion. Vidal et al. [43] proposed a model to estimate the width of cracks in the concrete due to pitting corrosion based on the experimental data resulting from two RC beam bars exposed to corrosion for 14 and 17 years. The model proposes the width of cracks as follows:

$$w_{cr} = k(\Delta A_s - \Delta A_{s0}) \quad (12)$$

Where k is a factor obtained from regression which equals 0.0575, ΔA_s is the steel loss of cross section due to corrosion and ΔA_{s0} is the loss of steel cross-section, which leads to the first crack. ΔA_s and ΔA_{s0} can be estimated by the following equations:

$$\Delta A_s = \frac{\pi}{4}(2\alpha x \emptyset_0 - \alpha^2 x^2) \quad (13)$$

$$\Delta A_{s0} = A_s[1 - \left[1 - \frac{\alpha}{\emptyset_0}\left(7.53 + 9.32\frac{c}{\emptyset_0}\right)10^{-3}\right]^2] \quad (14)$$

Where x is the pit depth, $\emptyset_0$ is the initial bar diameter, A_s is the initial area of the bar (mm^2), α is the pit concentration factor usually considered between 4 and 8, and c is the clear concrete cover (mm).

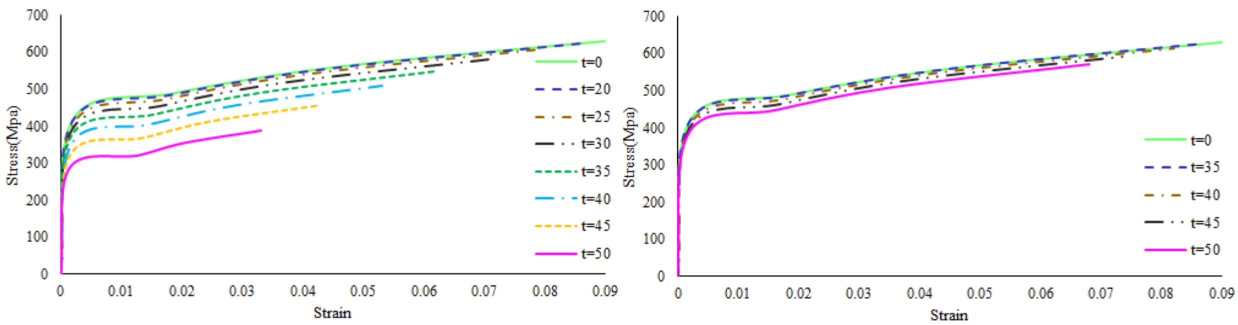

a) w/c ratio = 0.45 and t_{corr} = 16 years b) w/c ratio = 0.4 and t_{corr} = 31 years

Fig. 1. Time-dependent stress-strain curves of the bar under corrosion.

3.3. Changes in mechanical properties of reinforcement steel

Previous studies show that chloride-induced corrosion reduces steel bars' yield and ultimate stress and strain [44]. Kashani et al. reported that bars' ultimate strain and deformation are significantly reduced in corrosion scenarios with more than 15% mass loss [44]. They have shown that corrosion also changes the buckling collapse mechanism of the steel bars. Based on their study, corrosion with 10% mass loss leads to a 20% reduction in the buckling capacity of the steel bars in the corroded locations. Du et al. [45] investigated the deterioration of mechanical properties of steel bars under corrosion in an experimental study. They proposed the following Equation for the ultimate stress of corroded steel bars regardless of the type and size of the bars:

$$f = (1 - 0.005\Delta w) f_0 \quad (15)$$

Where f_0 is the ultimate stress of steel bars without corrosion and f is the ultimate stress of the corroded steel bars, Δw is the corrosion percentage that can be defined as follows:

$$\Delta w=\frac{A_0-A(t)}{A_0}\times 100 \tag{16}$$

Where A_0 is the initial cross-sectional area of the bar and $A(t)$ is the cross-sectional area of the bar at time t. Zhang et al. [46] investigated the impact of corrosion on the ultimate strain of steel and proposed the following Equation to estimate the ultimate strain in terms of corrosion percentage:

$$\varepsilon(t)=(1-0.0137\Delta w)\varepsilon_{u0} \tag{17}$$

In this Equation, $\varepsilon(t)$ is the ultimate strain of corroded steel and ε_{u0} is the ultimate strain of steel without corrosion. Figs.1a and 1b, obtained using the equations above, show stress-strain curves for steel bars with 25mm diameter under corrosion in concrete. The figures are drawn every five years for steel bars in concrete elements with w/c ratios of 0.40 and 0.45. it is also assumed that the concrete cover is 0.076 *m* according to the characteristics of the structure in section 4.
Table (1) shows that the corrosion initiation times for concretes with w/c of 0.4 and 0.45 are 31 and 16 years, respectively. Yield and ultimate stresses of the bars are fy = 420 MPa and fu = 630 MPa, respectively. After 50 years under corrosion, the pit depths for 25 mm bars in concretes with w/c ratios of 0.4, 0.45, and 0.5 have been obtained at 8, 14, and 18 mm, respectively. The cross-sectional areas of the bars in the concrete with different ratios of w/c are reduced from 490.8 mm^2 to 407, 267.18, and 148.3 mm^2. The yield stresses of the bars in the concrete with w/c ratios of 0.4, 0.45, and 0.5 are reduced from 420 MPa to 388, 287, and 51.5 MPa, respectively. The ultimate stresses of the bars in the concrete with different ratios of w/c are reduced from 630 MPa to 513.4, 371.1, and 213.95 MPa. The ultimate strains of steel bars in the concretes with w/c ratios of 0.4, 0.45, and 0.5 are reduced from 0.09 to 0.069, 0.033, and 0.004.

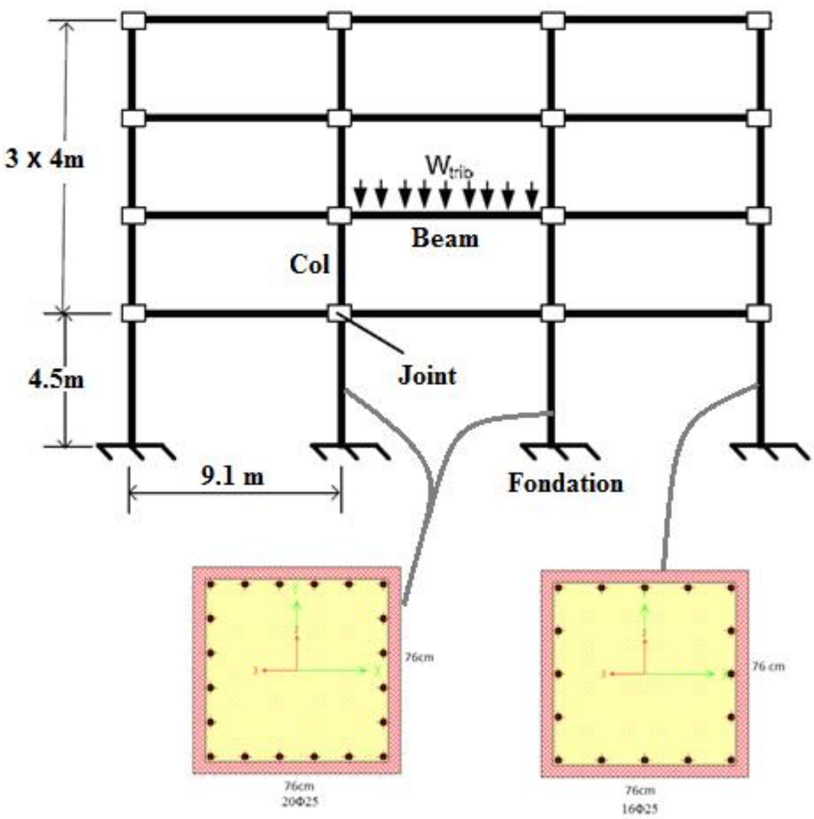

Fig. 2. The 4-story RC frame [46].

4. Moment frame under study

4.1. Moment frame geometry and loading

In this study, a 4-story (This model is one of the models Haselton designed) concrete frame was considered to investigate the impacts of corrosion on seismic performance of RC moment frames. The frame illustrated in Fig.2 has been designed according to ACI 318-05 and ASCE-SEI 7-05.
In this model, the compressive strength of pristine concrete is fc = 35 MPa. Steel bars' yield and ultimate stresses are 420 MPa and 630 MPa, respectively. The short-period spectral acceleration (SD_S) and 1.0-second spectral acceleration (SD_1) are 0.6g and 1.0g. This frame is modeled in OpenSees software, and the first period and Push-over curve for the structure are validated by Haselton et al. [47]. More details on this frame and its model can be found in Helston and Fema-p695 [48].

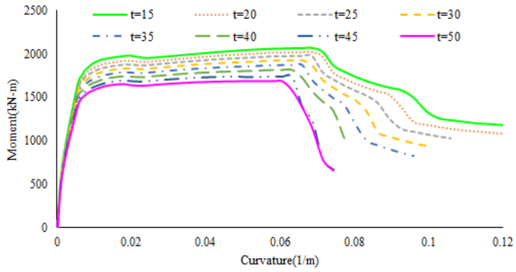

a) Corroded bars under pressure

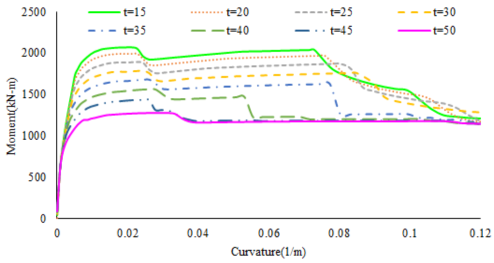

b) Corroded bars under tension

Fig. 3. Moment-curvature curves of the middle columns under the first corrosion scenario – w/c = 0.5.

In this study, it is assumed that the first-floor columns of the frame are exposed to two corrosion scenarios. In the first corrosion scenario, columns are exposed on one side, while columns are exposed on two sides in the second scenario.

4.2. Moment-curvature curves under corrosion

As shown in section 3, corrosion deteriorates the mechanical properties of concrete and steel reinforcement in RC structures, impacting the moment-curvature curve and behavior of RC elements. These impacts are considered through the equations presented in section 3 to obtain the moment-curvature curves. The effects of concrete confinement are also considered in the moment-curvature analysis. Since plastic hinges are defined in terms of moment-curvature diagrams, change in these curves leads to changes in plastic hinges' properties and nonlinear behavior. Therefore, chloride-induced corrosion changes the nonlinear behavior of plastic hinges, affecting the structure's seismic performance.

Fig.3 shows the moment-curvature curves for the interior columns of the first story constructed from the concrete with w/c=0.5during the building's lifecycle under the first corrosion scenario.
Similarly, for these sections and the primitive column sections, the calculations for moment-curvature diagrams, used for nonlinear analyses in OpenSees, were performed for all w/c ratios under both scenarios for each 5 years after the corrosion initiation.

4.3. Plastic joint model

In this study, plastic hinges are modeled at member ends using moment-curvature diagrams obtained in the previous section.

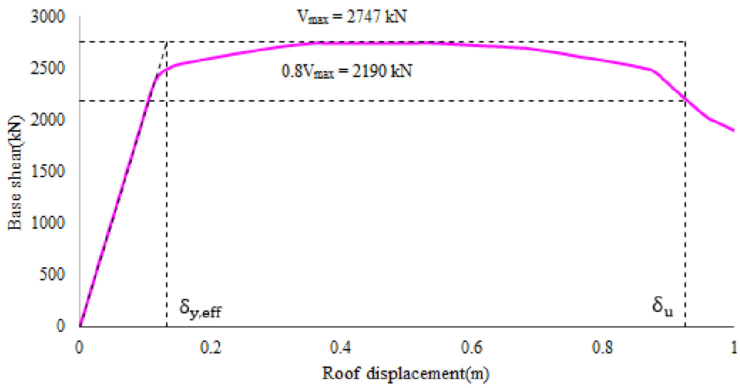

Fig. 4. The 4-story frame curve.

Research suggests that the Corley relationship provides an appropriate estimate for the plastic hinge length of elements with low axial loads. Therefore, the length of the plastic hinge is estimated using the Corley equation, as shown below [49]:

$$l_p=0.5d+0.2d\sqrt{d}\left(\frac{z}{d}\right) \tag{18}$$

Where *d* is the effective depth of the element (in *mm*), and *z* is the distance of the critical point from the contra-flexure point. The plastic hinge rotation in the final step can be obtained using the plastic hinge length as follows [50,51]:

$$\theta_p=(\varphi_u-\varphi_y)l_p \tag{19}$$

Where φ_u and φ_y are respectively yield and ultimate rotations, and l_p is the plastic hinge length. The moment-curvature diagrams are obtained by applying the impacts of corrosion on the material's properties. Under a corrosive environment over the building's lifecycle, the yield moment, ultimate moment, and the plastic curvature $(\varphi_u-\varphi_y)$ of sections reduced. The resulting moment-curvature diagrams for both corrosion scenarios at each time step are used in plastic hinges modeling for nonlinear static analysis and Incremental Dynamic Analysis (IDA) of corroded structural models.

5. Investigating the seismic performance of the concrete frame under various corrosion scenarios

5.1. Nonlinear static analysis

After obtaining moment-curvature curves for various corrosion conditions, the model's 4-story concrete frame is built using these curves at each period to investigate the seismic performances of this frame over its lifetime. Fig.4 shows the pushover curve for the frame, illustrating the base shear and ultimate displacement resulting from nonlinear analysis. V max is the maximum shear force obtained among all points. Also, the ultimate displacement, δ_u, is the roof displacement associated with 80% of maximum shear force (0.8V max). These parameters, δ_u and V_{max}, are used to calculate the over-strength factor, *Ω*, and ductility factor, *μ*; the strength factor is defined as follows:

$$\Omega=\frac{V_{max}}{V} \tag{20}$$

The base shear of the 4-story frame design is 875.4 KN. The ductility factor is defined as the ratio of the ultimate roof displacement, δ_u, to the effective roof yield displacement, $\delta_{y,eff}$:

$$\mu=\frac{\delta_u}{\delta_{y,eff}} \tag{21}$$

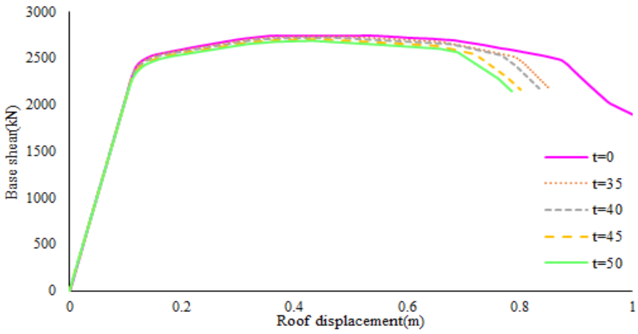

a) w/c = 0.40 and tcorr = 31 year.

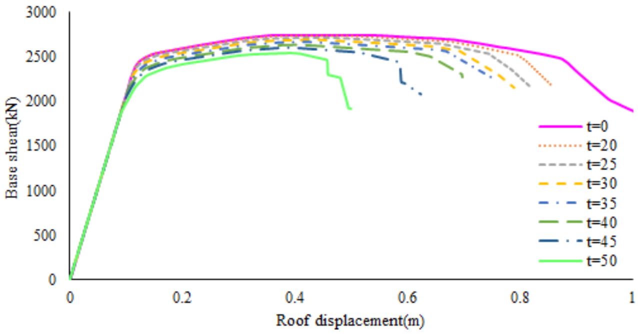

b) W/C = 0.45 & t_{corr}= 16.

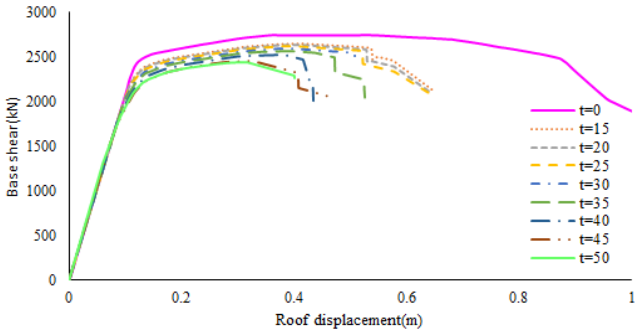

c) W/C = 0.50& t_{corr}= 10.

Fig. 5. The pushover curves for the 4-story concrete frame under the first corrosion scenario over its lifetime.

5.2. Nonlinear static analysis and structural performance curves

This section investigates the pushover curves resulting from nonlinear static analysis of the 4-story frame under various corrosion scenarios over its lifetime. Fig 5 shows the 4-story pushover curves of the frame over its lifetime for three w/c ratios of 0.4, 0.45, and 0.5 under the first corrosion scenario. Similarly, Fig. 6 shows the pushover curves for the second corrosion scenario.

5.3. Ductility and over-strength of the structure under corrosion

The over-strength and ductility are obtained from the pushover curves according to section 5.1.Fig.7a shows the strength factor reduction percentage, $(\Omega(t)\text{-}\Omega_0)/\Omega_0)$, for the 4-story frame under the corrosion scenarios for three w/c ratios.Fig.7b shows the ductility factors for the frame in the corrosion scenarios for three w/c ratios.Fig.7b illustrates a 50.19 and 63.72 percent reduction in the ductility of the frame with the w/c ratio of 0.5 after 50 years under the first and second corrosion scenarios, respectively. This figure also shows 10.86 and 22.36 percent reductions in the over-strength factors for the frame. The cutbacks in ductility and overstrength factors are also observed for other different w/c ratios over the frame's lifetime, illustrating the significant influence of chloride-induced corrosion on the ductility of the frame. This can be seen in other w/c ratios, showing that reduced ductility is the essential impact of corrosion due to chloride in the 4-story concrete frame.

In addition, Fig 7b. also shows that the increase of the w/c ratio from 0.40 to 0.50 leads to a significant reduction in the ductility of the frame at each period over its lifetime. For example, the increase of w/c ratio from 0.40 to 0.50 results in a 35.1 and 44.6 percent reduction in the ductility of the frame at the end of life of the frame. This shows the vital influence of the w/c ratio and the quality of concrete construction on the ductility of RC structures in coastal areas.

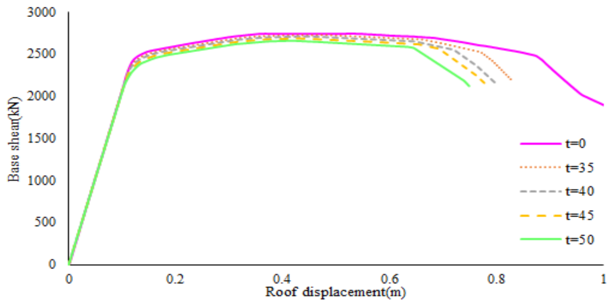

a) w/c = 0.40 and tcorr = 31.

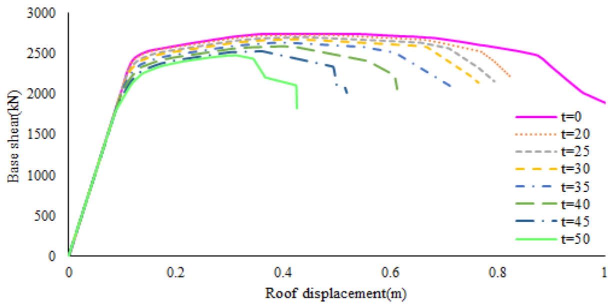

b) w/c = 0.45 and tcorr = 16.

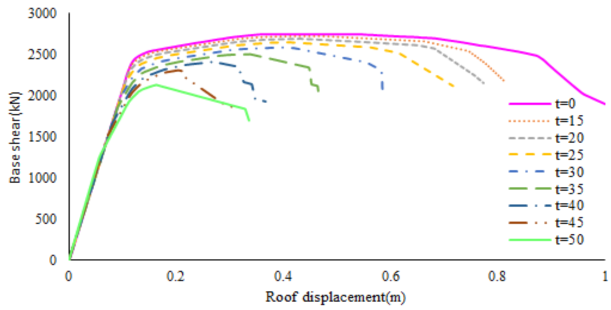

c) w/c = 0.50 and tcorr = 10.

Fig. 6. The pushover curves for a 4-story frame under the second corrosion scenario over its lifetime.

Fig. 7 illustrates that chloride-induced corrosion influences the ductility more than the overstrength in RC frames. Consequently, chloride-induced corrosion increases the probability of collapse of concrete structures due to reduced ductility.

5.4. Incremental dynamic analysis (IDA) of the frame under corrosion

This study uses Incremental Dynamic Analysis (IDA) with fixed steps to estimate the structure's seismic performance under chloride-induced corrosion. In this method, intensity measure (IM) can be either Peak Ground Acceleration (PGA) or spectral acceleration in the main period (Sa(T1)). In this study, the spectral acceleration in the main period of the structure (Sa(T1)) is considered as the earthquake intensity measure (IM). The advantage of the spectral acceleration in (Sa(T1)) compared to PGA is that Sa is related to the structure under study. Therefore, the characteristics of the structure are considered in the analysis. Also, the results of the analyses using (Sa(T1)) as the intensity measure show less dispersion.

The next step is determining Engineering Demand Parameters (EDP). In this study, the maximum drift is considered as the engineering demand. To analyze the structure, for each earthquake record, the spectral acceleration in the main period (for the 4-story frame in this study, the main period is 1.03 s) is obtained, and this spectral acceleration normalizes the record. Then, a suite of ground motion records is selected, and each record is scaled to several seismic intensity levels. Then, the records are applied to the structure to perform incremental dynamic analysis and compute the EDPs. Table (2) shows the 21 ground motion records used for IDA in this study. Since each record in the table has two horizontal components, 42 records are applied to the frame for IDA [48].

Fig.8.a shows IDA curves obtained using 42 records for the 4-story concrete frame in this study. Fig.8.b shows 16, 50, and 84%fractile IDA obtained using the records. The fractile curves summarize the damage measures and are used as lower bounds, central values, and upper bounds for responses. After applying the impacts of corrosion on the structural elements, new models are built and analyzed using IDA. One of IDA's most essential applications is obtaining fragility curves for structures. The following section presents fragility curve computations and probabilistic damage analyses.

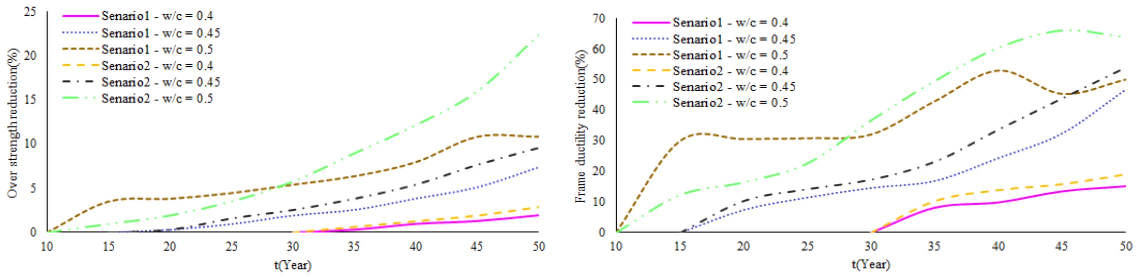

a) over-strength factor reduction. b) Frame ductility reduction percentage.

Fig. 7. Over strength and ductility reduction for the 4-story frame over its lifetime.

5.5. Fragility curves of the frame under study

Fragility curves show the conditional probability of a specified damage or damage state (DS) under a range of seismic intensities $P(DS|S_a)$. According to Hazus, fragility curves are assumed to be lognormal functions that describe damage state probabilities in terms of seismic intensities to obtain fragility curves [52]. Therefore, fragility curves are obtained using IDA curves as follows:

$$P(DS|Sa)=\Phi\left(\frac{1}{\beta_{DS}}\ln\left(\frac{S_a}{S_{a,\,DS}}\right)\right) \tag{22}$$

Where *DS* is the damage state (e.g., *DS1*, *DS2*, *DS3*, and *DS4*), *Sa* is the spectral acceleration of the fundamental structural mode, β_{DS} is the logarithmic standard deviation of the spectral acceleration in engineering demand associated with the damage level, $S_{a,\,DS}$ is the average spectral acceleration in engineering demand associated with the damage level in IDA curves, and φ is the standard normal cumulative distribution. BDS indicates the uncertainties in the problem that is considered as BDS (TOT0 = 0.5) based on FEMA P695. According to [53], for a 4-story moment frame concrete structure, four damage states are considered as follows:
1. Slight damage state (*DS1*) 2. Moderate damage state (*DS2*), 3. Severe damage (*DS3*) and 4. Collapse (*DS4*). According to Table 5.9a in Hazus, drifts for each damage sates of *DS1*, *DS2*, *DS3*, and *DS4* for the middle concrete moment frame are 0.0033, 0.0067, 0.02, and 0.053. These drifts are used in fragility analyses as the thresholds for specific damages.

Table 2. Records proposed by FEMA P695 [48].

ID No.	Earthquake			Recording Station	
	M	Year	Name	Name	Owner
1	6.7	1994	Northridge	Beverly Hills - Mulhol	USC
2	6.7	1994	Northridge	Canyon Country-WLC	USC
3	7.1	1999	Duzce, Turkey	Bolu	ERD
4	7.1	1999	Hector Mine	Hector	SCSN
5	6.5	1979	Imperial Valley	Delta	UNAMUCSD
6	6.5	1979	Imperial Valley	El Centro Array #11	USGS
7	6.9	1995	Kobe, Japan	Nishi-Akashi	CUE
8	6.9	1995	Kobe, Japan	Shin-Osaka	CUE
9	7.5	1999	Kocaeli, Turkey	Duzce	ERD
10	7.5	1999	Kocaeli, Turkey	Arcelik	KOERI
11	7.3	1992	Landers	Yermo Fire Station	CDMG
12	7.3	1992	Landers	Coolwater	SCE
13	6.9	1989	Loma Prieta	Capitola	CDMG
14	6.9	1989	Loma Prieta	Gilroy Array #3	CDMG
15	7.4	1990	Manjil, Iran	Abbar	BHRC
16	6.5	1987	Superstition Hills	El Centro Imp. Co.	CDMG
17	6.5	1987	Superstition Hills	Poe Road (temp)	USGS
18	7.0	1992	Cape Mendocino	Rio Dell Overpass	CDMG
19	7.6	1999	Chi-Chi, Taiwan	CHY101	CWB
20	7.6	1999	Chi-Chi, Taiwan	TCU045	CWB
21	6.6	1971	San Fernando	LA - Hollywood Stor	CDMG
22	6.5	1976	Friuli, Italy	Tolmezzo	--

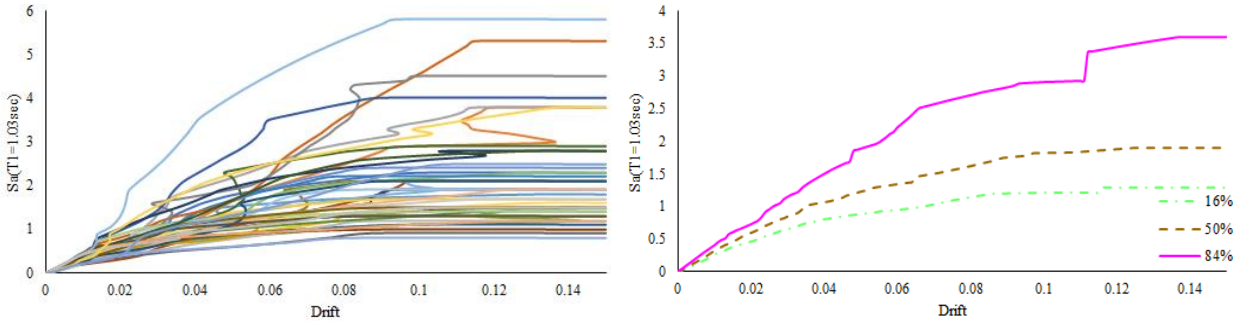

a) Under the records of Table 2. b) Curves at 16, 50 and 84%.

Fig. 8. IDA curves of the 4-story concrete frame.

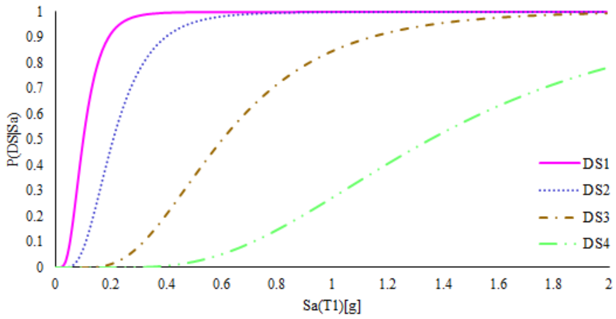

Fig. 9. Fragility curves obtained for a 4-story concrete frame.

As shown in Fig. 9, the pristine structure, without considering the impacts of corrosion, exceeds the slight (DS1) and moderate (DS2) damage states for both the DBE and MCE earthquakes. In other words, the pristine and corroded structures reach the DS1 and DS2 damage states. Therefore, the impacts of corrosion on fragility curves at these damage states (DS1 and DS2) will not be studied. Fig. 9 shows the fragility curves of this study's 4-story concrete moment frame. This figure shows the probability of exceeding the damage states for design basis earthquake (DBE) and the Maximum Considered Earthquake (MCE). As pointed out, the site design spectral accelerations at short and 1-second periods are SD_S = 1.0g and SD_1 = 0.60g, respectively. Also, SD_1 and SD_S for the Maximum Considered Earthquake (MCE) are 1.5g and 0.90g, respectively [48]. According to the values of SD_S and SD_1 for DBE and MCE, the spectral acceleration of the 4-story concrete frame at DBE and MCE are 0.58g and 0.87g, respectively. At the DBE intensity level, the frame's response indicates a probability of 45% exceeding DS3 and a probability of 4% exceeding DS4 (Fig. 9). At the MCE intensity level, the frame's response indicates a probability of 76.4% exceeding DS3 and a probability of 17.9% exceeding DS4 (Fig. 9). In the next section, after applying the impacts of corrosion on the structure under two scenarios and three w/c ratios, IDA and fragility analyses are performed every five years after corrosion initiation time. Then, the probability of exceeding the damage states of DS3 and DS4, given the seismic intensity level, is investigated.

5.6. The Impact of various corrosion scenarios on fragility curves

This section investigates the impacts of corrosion on the fragility curves under various corrosion conditions at the DBE and MCE. Figs.10 shows the fragility curves for the 4-story frame over its lifetime for three w/c ratios of 0.40, 0.45, and 0.50 under the first corrosion scenario. Similarly, Figs.11a-f shows the fragility curves for the frame under the second corrosion scenario. It should be noted that these curves are calculated for DS3 and DS4. Fig. 10 also indicates that corrosion has influenced the fragility curves related to DS4 (e.g., collapse) more than DS4.

Figs. 10 and 11 give us the following conclusion:

At the DBE, under the first corrosion scenario, the probability of exceeding DS3 at the end of the service lifetime increases from 46.37% to 48.66%, 52.24%, and 53.53%for the concrete structures with w/c ratios of 0.40, 0.45, and 0.50, respectively. In other words, after 50 years, the probabilities of exceeding DS3 for the frames constructed from concretes with the w/c ratios of 0.40, 0.45, and 0.50 increase by 2.3%, 5.87%, and 7.16%, respectively. Also, in this condition, the probability of exceeding DS4 at the end of the service lifetime increases from 4.18% to 5.66%, 10.33%, and 13.33%. In other words, after 50 years, the probabilities of exceeding DS4 for the frames constructed from concretes with the w/c ratios of 0.40, 0.45, and 0.50 increase by 1.49%, 6.15%, and 9.15%, respectively.

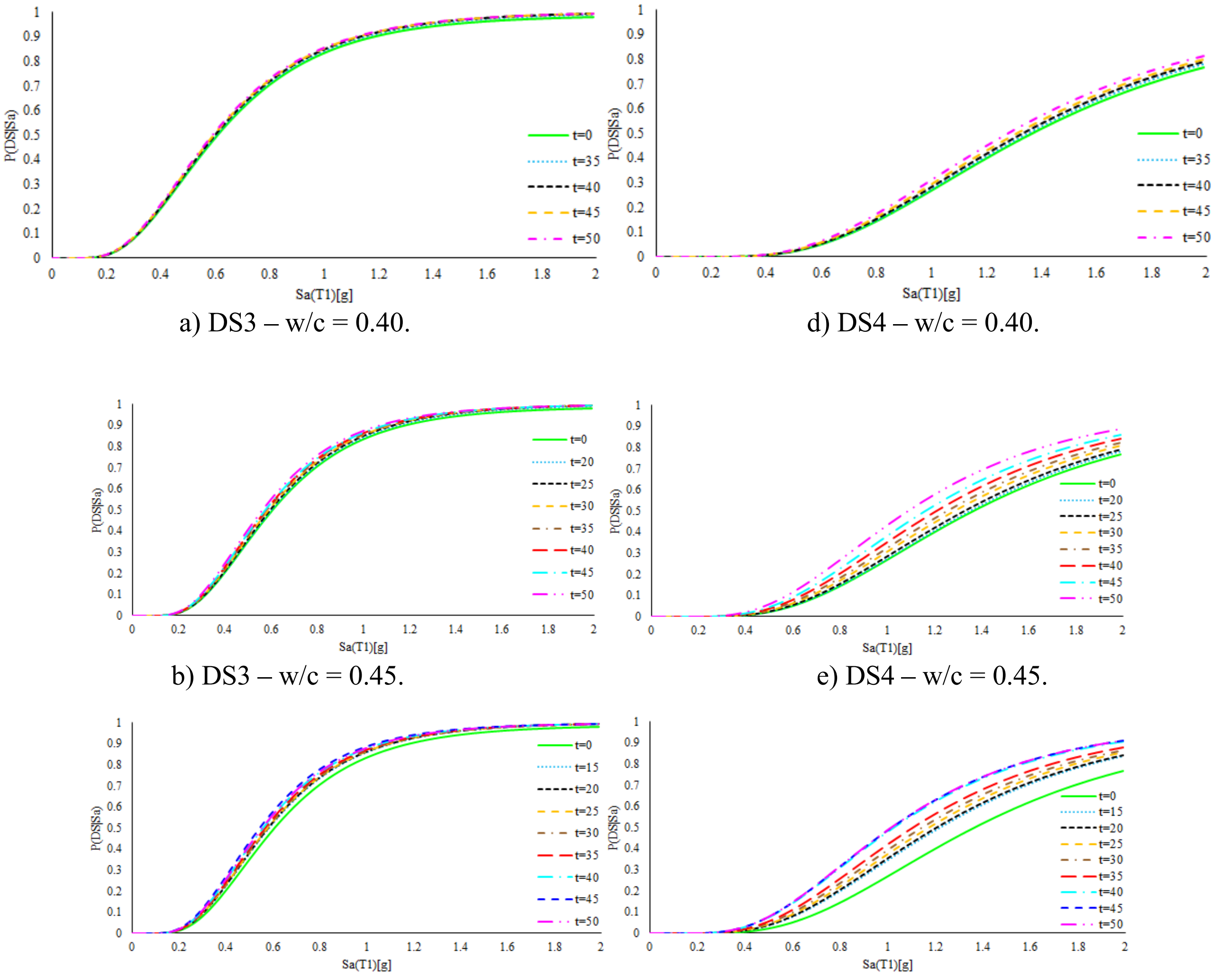

a) DS3 – w/c = 0.40. d) DS4 – w/c = 0.40.

b) DS3 – w/c = 0.45. e) DS4 – w/c = 0.45.

c) DS3 – w/c = 0.50. f) DS4 – w/c = 0.5.

Fig. 10. Fragility curves of the 4-story frame under the first corrosion scenario.

At the MCE intensity, under the first corrosion scenario, the probability of exceeding DS3 at the end of the service lifetime increases from 76.42% to 78.15%, 80.71%, and 81.58% for the concrete structures with w/c ratios of 0.40, 0.45, and 0.50, respectively. In other words, after 50 years, the probabilities of exceeding DS3 for the frames constructed from concretes with the w/c ratios of 0.40, 0.45, and 0.50 increase by 1.73%, 4.3%, and 5.16%, respectively. Also, in this condition, the probability of exceeding DS4 at the end of the service lifetime increases from 17.91% to 21.98%, 32.56%, and 37.86%. In other words, after 50 years, the probabilities of exceeding DS4 for the frames constructed from concretes with the w/c ratios of 0.40, 0.45, and 0.50 increase by 4.07%, 14.65%, and 19.95%, respectively.

Under the second corrosion scenario at the DBE intensity level, the probability of exceeding DS3 at the end of the service lifetime increases from 46.37% to 49.82%, 55.2%, and 96.11% for the concrete structures with w/c ratios of 0.40, 0.45, and 0.50, respectively. In other words, after 50 years, the probabilities of exceeding DS3 for the frames constructed from concretes with the w/c ratios of 0.40, 0.45, and 0.50 increase by 3.45%, 8.83%, and 49.74%, respectively. For the concrete frame with w/c ratios of 0.50 in the last five years of the structure's lifetime, a significant increase in the probability of exceeding DS3 is observed (Fig 11. f).

Under the second corrosion scenario at the DBE intensity level, the probability of exceeding DS4 at the end of the service lifetime increases from 4.18% to 6.92%, 13.99%, and 81.27%for the concrete structures with w/c ratios of 0.40, 0.45, and 0.50, respectively. In other words, after 50 years, the probabilities of exceeding DS3 for the frames constructed from concretes with the w/c ratios of 0.40, 0.45, and 0.50 increase by 2.74%, 9.81%, and 77.09%, respectively. For the concrete frame with w/c ratios of 0.50 in the last five years of the structure's lifetime, a significant increase in the probability of exceeding DS3 (77.09%) is observed (Fig 11. f). In this case, the probability of collapse under an earthquake is significant.

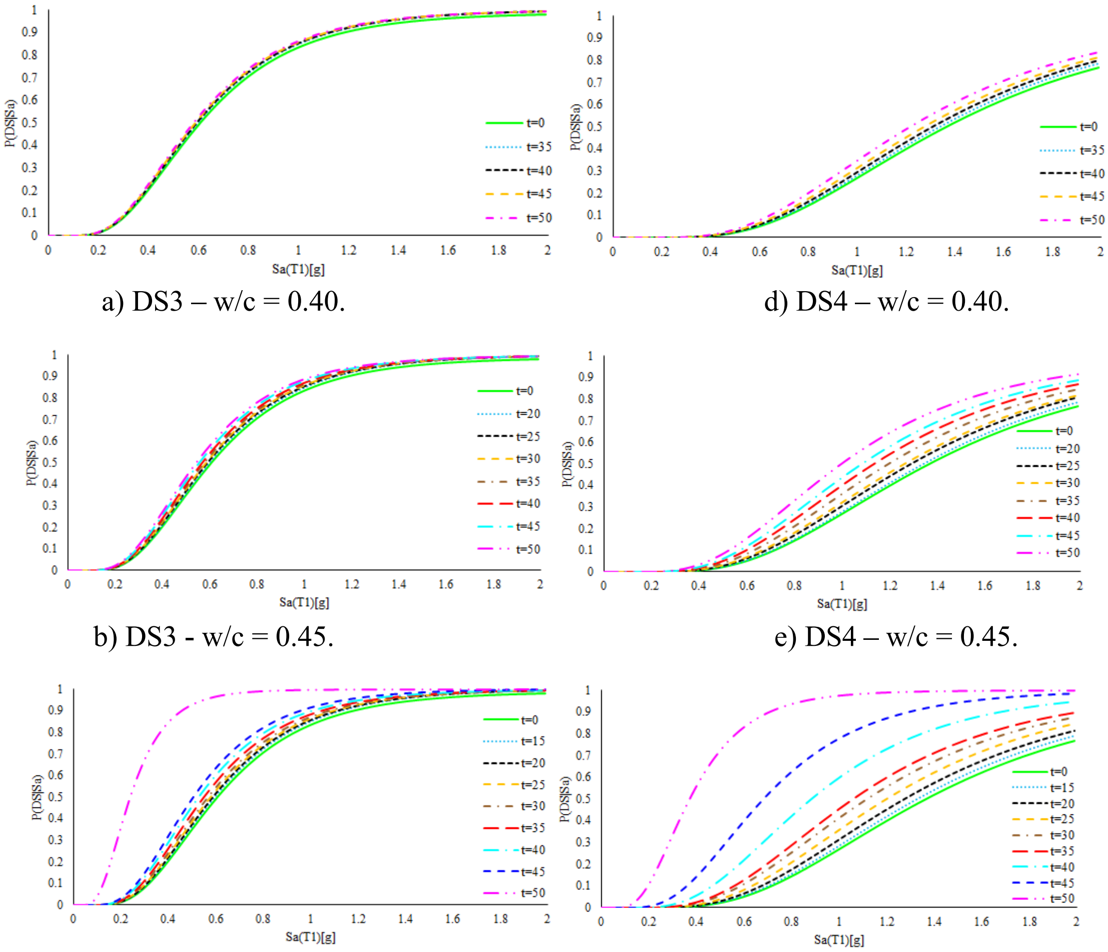

a) DS3 – w/c = 0.40. d) DS4 – w/c = 0.40.

b) DS3 - w/c = 0.45. e) DS4 – w/c = 0.45.

c) DS3 – w/c = 0.50. f) DS4 – w/c = 0.50.

Fig. 11. Fragility curves of the 4-story concrete frame under the second corrosion scenario.

Under the second corrosion scenario at the MCE intensity level, the probability of exceeding DS3 at the end of the service lifetime increases from 76.42% to 79%, 82.68%, and 99.49%for the concrete structures with w/c ratios of 0.40, 0.45, and 0.50, respectively. In other words, after 50 years, the probabilities of exceeding DS3 for the frames constructed from concretes with the w/c ratios of 0.40, 0.45, and 0.50 increase by 2.58%, 6.26%, and 23.7%, respectively.

Under the second corrosion scenario at the MCE intensity level, the probability of exceeding DS4 at the end of the service lifetime increases from 17.91% to 25.12, 39.37, and 95.53%for the concrete structures with w/c ratios of 0.40, 0.45, and 0.50, respectively. In other words, after 50 years, the probabilities of exceeding DS3 for the frames constructed from concretes with the w/c ratios of 0.40, 0.45, and 0.50 increase by 7.21, 21.46, and 77.62%, respectively. For the concrete frame with w/c ratios of 0.50 in the last five years of the structure's lifetime, a significant increase in the probability of exceeding DS4 (95.53%) is observed (Fig 11. f).In this case, the probability of collapse of the corroded frame under an earthquake is close to 100%.

6. Conclusion

This paper investigates the impact of corrosion on the seismic fragility of concrete moment frames. To achieve this, the analysis begins by evaluating the mechanism of corrosion initiation and its effects on the mechanical properties of concrete and steel bars. Considering these corrosion effects, time-dependent moment-curvature diagrams are obtained for the first-story columns over the structure's lifetime. For each water-to-cement (w/c) ratio (0.40, 0.45, and 0.50), corrosion initiation time is estimated probabilistically using meta-exploratory methods based on HL-M. Finally, the seismic capacity, ductility, and seismic fragility of frames constructed from concretes with the three w/c ratios are investigated under two corrosion scenarios using nonlinear static and Incremental Dynamic Analyses (IDA).

The results of this study can be briefly summarized as follows:

1. Under two scenarios, the study investigated the seismic capacity reduction due to corrosion at the end of service life. For concrete frames with water-to-cement (w/c) ratios of 0.40, 0.45, and 0.50, the first scenario resulted in reductions of 1.92%, 7.35%, and 10.86% in seismic capacity, respectively. Under the second scenario, the reductions were more pronounced, reaching 2.88%, 9.58%, and 22.36% for the respective w/c ratios. We can observe a clear trend of increasing seismic capacity reduction with higher w/c ratios and more severe corrosion (scenario 2).

2. Under the first corrosion scenario, the ductility of the frames constructed from concretes the w/c ratios of 0.40, 0.45, and 0.50 reduces by 15.3%, 46.97%, and 50.19%, respectively. The seismic capacity under the second scenario for the concrete frames with the w/c ratios of 0.40, 0.45, and 0.50 was reduced by 19.07%, 54%, and 63.71%, respectively.

3. The probability of exceeding extensive structural damage (DS3) for the pristine concrete frame the DBE intensity level is 46.37%. At the end of the service lifetime under the first corrosion scenario, the probabilities of exceeding DS3 for w/c ratios of 0.40, 0.45, and 0.50 increase to 48.6%, 52.34%, and 53.52%, respectively. Under the second corrosion scenario, for the same w/c ratios, the probabilities of exceeding DS3 increase to 49.8%, 55.2%, and 96.11%.

4. The probability of exceeding DS3 for the frame at the MCE intensity level before corrosion initiation is 76.42%. At the end of the service lifetime under the first corrosion scenario, the probabilities of exceeding DS3 for w/c ratios of 0.40, 0.45, and 0.50 increase to 78.15%, 80.71%,

and 81.58%, respectively. Under the second corrosion scenario, for the same w/c ratios, the probabilities of exceeding DS3 increase to 79%, 82.68%, and 99.49%.

5. The probability of exceeding complete structural damage (DS4) at the DBE before corrosion initiation is 4.18%. At the end of the service lifetime under the first corrosion scenario, for w/c ratios of 0.40, 0.45, and 0.50, this probability increases to 5.66, 10.33, and 13.13%, respectively. Under the second corrosion scenario, for the same w/c ratios, this probability increases to 6.92, 13.99, and 81.21%, respectively.

6. The probability of exceeding DS4 at the MCE before corrosion initiation is 17.91%. At the end of the service lifetime under the first corrosion scenario, for w/c ratios of 0.40, 0.45, and 0.50, this probability increases to 21.98%, 32.56%, and 37.86%, respectively. Under the second corrosion scenario, for the same w/c ratios, this probability increases to 25.12%, 39.37%, and 95.53%.

Funding

No funding was received to assist with the preparation of this manuscript.

Conflict of interest

The authors have no competing interests to declare relevant to this article's content.

Authors contribution statement

Mohammad Amiri: Conceptualization, Data curation, Formal analysis, Investigation, Methodology, Resources, Software, Visualization, Writing - original draft.

Amirhossein Jafary: Corresponding Author, Conceptualization, Data curation, Formal analysis, Investigation, Methodology, Resources, Software, Visualization, Writing - original draft.

Ali khodam: Conceptualization, Data curation, Formal analysis, Investigation, Methodology, Resources, Software, Visualization, Writing - original draft.

Mohsenali Shayanfar: Project administration, Resources, Supervision.

Sajad Zarei: Conceptualization, Data curation, Formal analysis, Investigation, Methodology, Resources, Software, Visualization, Writing - original draft.

References

[1] Jafary A, Shayanfar MA, Ghanooni-Bagha M. Investtigation on the corrosion initiation time of reinforced concrete structures in different distances from the sea. Amirkabir J Civ Eng 2023;55:8.

[2] Ghanooni-Bagha M, YekeFallah MR, Shayanfar MA. Durability of RC structures against carbonation-induced corrosion under the impact of climate change. KSCE J Civ Eng 2020;24:131–42.

[3] Neville A. Chloride attack of reinforced concrete: an overview. Mater Struct 1995;28:63–70.

[4] Karimi A, Ghanooni-Bagha M, Ramezani E, Shirzadi Javid AA, Zabihi Samani M. Influential factors on concrete carbonation: a review. Mag Concr Res 2023;75:1212–42.

[5] Ghanooni-Bagha M, Shayanfar MA, Shirzadi-Javid AA, Ziaadiny H. Corrosion-induced reduction in compressive strength of self-compacting concretes containing mineral admixtures. Constr Build Mater 2016;113:221–8.

[6] Goharrokhi A, Ahmadi J, Shayanfar MA, Ghanooni-Bagha M, Nasserasadi K. Effect of transverse reinforcement corrosion on compressive strength reduction of stirrup-confined concrete: an experimental study. Sādhanā 2020;45:1–9.

[7] Alinaghimaddah S, Shayanfar MA, Ghanooni-Bagha M. Effect of distance from the sea on reinforced concrete chloride corrosion probability. AUT J Civ Eng 2020;4:199–208.

[8] Poulsen E, Mejlbro L. Diffusion of chloride in concrete: theory and application. CRC Press; 2010.

[9] Nouri Y, Ghanbari MA, Fakharian P. An integrated optimization and ANOVA approach for reinforcing concrete beams with glass fiber polymer. Decis Anal J 2024;11:100479. doi:10.1016/j.dajour.2024.100479.

[10] Biondini F, Palermo A, Toniolo G. Seismic performance of concrete structures exposed to corrosion: case studies of low-rise precast buildings. Struct Infrastruct Eng 2011;7:109–19.

[11] Ghanooni-Bagha M, Zarei S, Savoj HR, Shayanfar MA. Time-dependent seismic performance assessment of corroded reinforced concrete frames. Period Polytech Civ Eng 2019;63:631–40.

[12] Tuutti K. Corrosion of steel in concrete. Cement-och betonginst.; 1982.

[13] Shayanfar MA, Barkhordari MA, Ghanooni-Bagha M. Estimation of corrosion occurrence in RC structure using reliability based PSO optimization. Period Polytech Civ Eng 2015;59:531–42.

[14] Di Sarno L, Pugliese F. Numerical evaluation of the seismic performance of existing reinforced concrete buildings with corroded smooth rebars. Bull Earthq Eng 2020;18:4227–73.

[15] Shayanfar MA, Safiey A. A new approach for nonlinear finite element analysis of reinforced concrete structures with corroded reinforcements. Comput Concr 2008;5.

[16] Du YG, Clark LA, Chan AHC. Effect of corrosion on ductility of reinforcing bars. Mag Concr Res 2005;57:407–19.

[17] Val D V, Melchers RE. Reliability of deteriorating RC slab bridges. J Struct Eng 1997;123:1638–44.

[18] Lee H-S, Noguchi T, Tomosawa F. Evaluation of the bond properties between concrete and reinforcement as a function of the degree of reinforcement corrosion. Cem Concr Res 2002;32:1313–8.

[19] Inci P, Goksu C, Ilki A, Kumbasar N. Effects of reinforcement corrosion on the performance of RC frame buildings subjected to seismic actions. J Perform Constr Facil 2013;27:683–96.

[20] Simioni P. Seismic response of reinforced concrete structures affected by reinforcement corrosion. Technische Universität Braunschweig, 2009.

[21] Afsar Dizaj E, Madandoust R, Kashani MM. Exploring the impact of chloride-induced corrosion on seismic damage limit states and residual capacity of reinforced concrete structures. Struct Infrastruct Eng 2018;14:714–29.

[22] Di Sarno L, Pugliese F. Seismic fragility of existing RC buildings with corroded bars under earthquake sequences. Soil Dyn Earthq Eng 2020;134:106169.

[23] Ghanooni-Bagha M. Influence of chloride corrosion on tension capacity of rebars. J Cent South Univ 2021;28:3018–28.

[24] Hasandoost AA, Karimi A, Shayanfar MA, Ghanooni-Bagha M. Probabilistic evaluation of chloride-induced corrosion effects on design parameters of RC beams. Eur J Environ Civ Eng 2023:1–15.

[25] Jafary A, Zaherbin P, Ghanooni-Bagha M, Shayanfar M. Collapse assessment of high-rise reinforced concrete building under chloride induced pitting corrosion subjected to near-field and far-field ground motions. Sādhanā 2023;48:182.

[26] Yalciner H, Sensoy S, Eren O. Seismic performance assessment of a corroded 50-year-old reinforced concrete building. J Struct Eng 2015;141:5015001.

[27] Vaezi H, Karimi A, Shayanfar M, Safiey A. Seismic performance of low-rise reinforced concrete moment frames under carbonation corrosion. Earthquakes Struct 2021;20:215–24.

[28] Richardson MG. Fundamentals of durable reinforced concrete. CRC Press; 2002.

[29] Berke NS, Hicks MC. Estimating the life cycle of reinforced concrete decks and marine piles using laboratory diffusion and corrosion data. Corros. forms Control Infrastruct., ASTM International; 1992.

[30] Takewaka K, Mastumoto S. Quality and cover thickness of concrete based on the estimation of chloride penetration in marine environments. Spec Publ 1988;109:381–400.

[31] Bamforth PB, Price WF, Emerson M. International Review of Chloride Ingress Into Structural Concrete: A Trl Report (Trl 359) 1997.

[32] McGee R. Modelling of durability performance of Tasmanian bridges. ICASP8 Appl Stat Probab Civ Eng 1999;1:297–306.

[33] Papadakis VG, Roumeliotis AP, Fardis MN, Vagenas CG. Mathematical modelling of chloride effect on concrete durability and protection measures. Concr Repair, Rehabil Prot 1996:165–74.

[34] Vu KAT, Stewart MG. Structural reliability of concrete bridges including improved chloride-induced corrosion models. Struct Saf 2000;22:313–33.

[35] Ghosh J, Padgett JE. Aging considerations in the development of time-dependent seismic fragility curves. J Struct Eng 2010;136:1497–511.

[36] Stewart MG, Rosowsky D V. Structural safety and serviceability of concrete bridges subject to corrosion. J Infrastruct Syst 1998;4:146–55.

[37] Stewart MG, Rosowsky D V. Time-dependent reliability of deteriorating reinforced concrete bridge decks. Struct Saf 1998;20:91–109.

[38] Li CQ. Life-cycle modeling of corrosion-affected concrete structures: propagation. J Struct Eng 2003;129:753–61.

[39] Vidal T, Castel A, Francois R. Corrosion process and structural performance of a 17 year old reinforced concrete beam stored in chloride environment. Cem Concr Res 2007;37:1551–61.

[40] Yuan Y, Jiang J, Peng T. Corrosion Process of Steel Bar in Concrete in Full Lifetime. ACI Mater J 2010;107.

[41] Liu T, Weyers RW. Modeling the dynamic corrosion process in chloride contaminated concrete structures. Cem Concr Res 1998;28:365–79.

[42] Vecchio FJ, Collins MP. The modified compression-field theory for reinforced concrete elements subjected to shear. ACI J 1986;83:219–31.

[43] Vidal T, Castel A, François R. Analyzing crack width to predict corrosion in reinforced concrete. Cem Concr Res 2004;34:165–74.

[44] Kashani MM, Crewe AJ, Alexander NA. Nonlinear stress–strain behaviour of corrosion-damaged reinforcing bars including inelastic buckling. Eng Struct 2013;48:417–29.

[45] Du YG, Clark LA, Chan AHC. Residual capacity of corroded reinforcing bars. Mag Concr Res 2005;57:135–47.

[46] Zhang PS, Lu M, Li XY. The mechanical behaviour of corroded bar. J Ind Build 1995;25:41–4.

[47] Haselton CB, Liel AB, Dean BS, Chou JH, Deierlein GG. Seismic collapse safety and behavior of modern reinforced concrete moment frame buildings. Struct. Eng. Res. Front., 2007, p. 1–14.

[48] Fema-p695. Quantification of building seismic performance factors. US Department of Homeland Security, FEMA; 2009.

[49] Zhao X, Wu Y-F, Leung AY, Lam HF. Plastic hinge length in reinforced concrete flexural members. Procedia Eng 2011;14:1266–74.

[50] Lehman DE. Seismic performance of well-confined concrete bridge columns. University of California, Berkeley; 1998.

[51] Mortezaei A. Plastic hinge length of RC columns under the combined effect of near-fault vertical and horizontal ground motions. Period Polytech Civ Eng 2014;58:243–53.

[52] Ghasemi Jouneghani H, Nouri Y, Mortazavi M, Haghollahi A, Memarzadeh P. Seismic Performance Factors of Elliptic-Braced Frames with Rotational Friction Dampers through IDA. Pract Period Struct Des Constr 2024;29:1–24. doi:10.1061/PPSCFX.SCENG-1540.

[53] Hazus-MH-2.1. Hazus-MH 2.1 Canada, User and Technical Manual: Earthquake Module. Natural Resources Canada Ottawa, ON, Canada; 2014.